Segmentation of aorta and main pulmonary artery of non-contrast CT images using U-Net for chronic thromboembolic pulmonary hypertension: Evaluation of robustness to contacts with blood vessels

Hidenobu Suzuki [a], Mikio Matsuhiro [a], Yoshiki Kawata [a], Toshihiko Sugiura [b], Nobuhiro Tanabe [b], Masahiko Kusumoto [c], Masahiro Kaneko [d], Noboru Niki [e]

[a] Graduate School of Technology, Industrial and Social Sciences, Tokushima University, Tokushima, Japan; [b] Department of Respirology, Chiba University, Chiba, Japan; [c] Department of Diagnostic Radiology, National Cancer Center Hospital, Tokyo, Japan; [d] Tokyo Health Service Association, Tokyo, Japan; [e] Medical Science Institute Inc., Tokushima, Japan

ABSTRACT

Enlargement of the pulmonary artery is a morphological abnormality of pulmonary hypertension patients. Diameters of the aorta and main pulmonary artery (MPA) are useful for predicting the presence of pulmonary hypertension. A major problem in the automatic segmentation of the aorta and MPA from non-contrast CT images is the invisible boundary caused by contact with blood vessels. In this study, we applied U-Net to the segmentation of the aorta and MPA from non-contrast CT images for normal and chronic thromboembolic pulmonary hypertension (CTEPH) cases and evaluated the robustness to the contacts between blood vessels. Our approach of the segmentation consists of three steps: (1) detection of trachea branch point, (2) cropping region of interest centered to the trachea branch point, and (3) segmentation of the aorta and MPA using U-Net. The segmentation performances were compared in seven methods: 2D U-Net, 2D U-Net with pre-trained VGG-16 encoder, 2D U-Net with pre-trained VGG-19 encoder, 2D Attention U-Net, 3D U-Net, an ensemble method of them, and our conventional method. The aorta and MPA segmentation methods using these U-Net achieved higher performance than a conventional method. Although the contact boundaries of blood vessels caused lower performance compared with the non-contact boundaries, the mean boundary distances were below about one pixel.

Keywords: Chronic thromboembolic pulmonary hypertension, computed tomography, contact surface ratio, U-Net

1. INTRODUCTION

Enlargement of the pulmonary artery is a morphological abnormality of pulmonary hypertension patients. Diameters of the aorta and main pulmonary artery (MPA) are useful for predicting the presence of pulmonary hypertension [1]-[4]. Several methods for automatic segmentation of aorta and MPA of non-contrast CT images have been proposed. Kurugol et al. [5],[6] proposed an automated aorta segmentation and aortic calcification detection method using circular Hough transformation and three-dimensional level sets. Xie et al. [7],[8] proposed an automated aorta and pulmonary trunk segmentation method using a cylinder-tracking algorithm, pre-computed anatomy label maps, and refinement by a triangular mesh model. Gamechi et al. [9],[10] proposed the aorta and main pulmonary artery segmentation using optimal surface graph cuts and the multi-atlas registration method. They also proposed an aortic diameter measurement method at multiple cross-sectional slices perpendicular to the aortic centerline. Suzuki et al. [11] proposed a segmentation method using mediastinal vascular centerlines and the probabilistic atlases of the aorta and MPA. They also proposed a three-dimensional measurement method of the vascular diameters. A major problem in the automatic segmentation of the aorta and MPA from non-contrast CT images is the invisible boundary caused by contact with blood vessels. However, the segmentation performance focused on the contact parts has not been evaluated. In this study, we applied U-Net [12],[13] to the segmentation of the aorta and MPA from non-contrast CT images for normal and chronic thromboembolic pulmonary hypertension (CTEPH) cases. Furthermore, we evaluated their robustness to the contacts of the blood vessels.

Medical Imaging 2022: Computer-Aided Diagnosis, edited by Karen Drukker, Khan M. Iftekharuddin, Hongbing Lu, Maciej A. Mazurowski, Chisako Muramatsu, Ravi K. Samala, Proc. of SPIE Vol. 12033, 1203325 · © 2022 SPIE · 1605-7422 · doi: 10.1117/12.2612705

2. MATERIALS AND METHODS

2.1 Non-contrast CT image datasets

This study used two datasets of non-contrast chest CT images: normal cases (dataset A) and CTEPH cases (dataset B). Collection and analysis of data were approved by the Institutional Review Board at these institutions. The CT images of dataset A were acquired on Aquilion Lightning scanner with 30 mA at 120 kVp, plane resolution: 0.625 mm, reconstruction matrix: 512 x 512, convolution kernel: FC01, slice thickness: 1.0 mm, and reconstruction interval: 1.0 mm. The CT images of dataset B were acquired on Aquilion ONE scanner with 112-295 mA at 120 kVp, plane resolution: 0.570-0.698 mm, reconstruction matrix: 512 x 512, convolution kernel: FC07, slice thickness: 0.5 mm, and reconstruction interval: 0.5 mm. The number of cases in datasets A and B was 100 and 24.

2.2 Manual annotation of ground truth

Manual annotation of the ground truth of the aorta and main pulmonary artery was performed separately in the axial plane. The vertical interval of this annotation was 10 slices. The window level and width for the annotation were adjusted to 50 and 300, respectively. Manual annotation of contact boundary pixels in the aorta was performed for each ground truth slice as shown in Fig. 2. This annotation consisted of three types: contacts of the aorta with MPA, contacts of the aorta with vena cava, and contact of the aorta with the esophagus. Contact surface ratios (CSR) were calculated as a ratio of contact boundary pixels per whole boundary pixels.

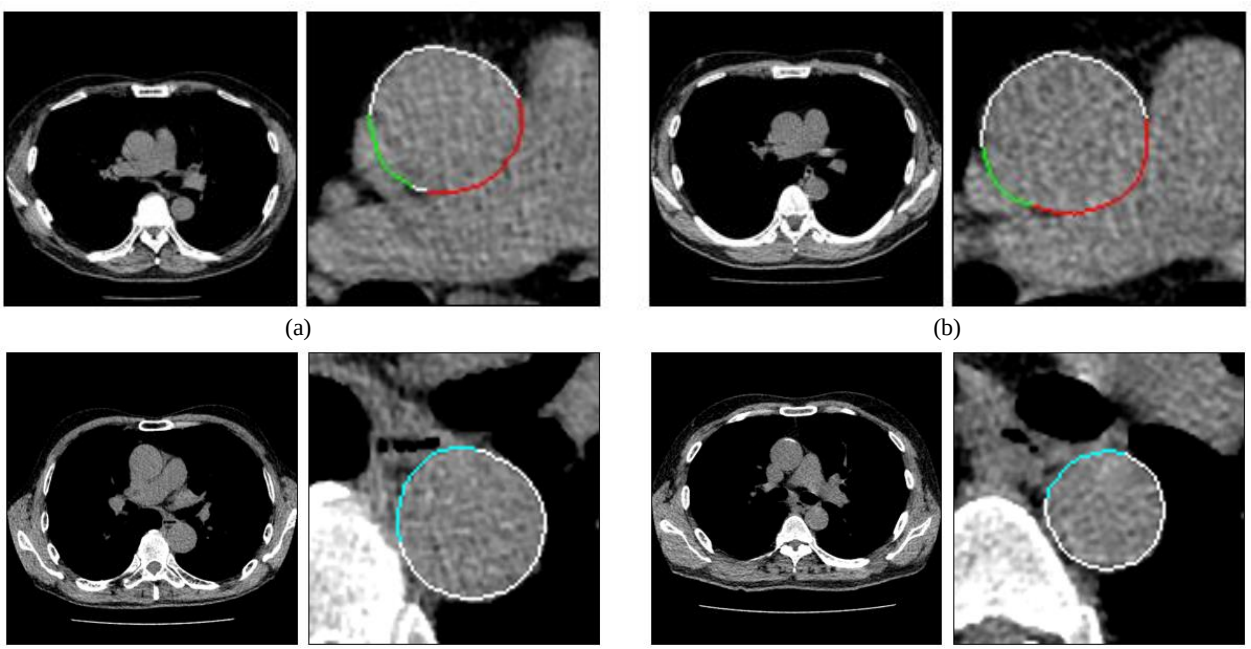

Fig. 1. Manual annotation results of non-contact and contact boundaries of ascending aorta (a),(b) and descending aorta (c),(d). Red, green, and blue colors show contact boundaries: a boundary of the aorta with main pulmonary artery, a boundary of the aorta with vena cava, and a boundary of aorta with esophagus. Contact surface ratios (*CSR*) in (a) and (b) were 53.1% and 51.9%, respectively. *CSRs* in (c) and (d) were 31.7% and 33.6%, respectively.

2.3 Cropping region of interest centered to trachea branch point

Region of interest (ROI) centered to a trachea branch point is cropped from the original CT volume as follows. First, body, bone, lungs, and airway were segmented using our previous methods using intensity and anatomical features [14][15]. Then, the centerline of the airway was extracted by a thinning method. The centerline was classified into three classes based on the anatomical position: trachea, right bronchus, and left bronchus. Finally, ROI centered to the cross point of three branches was cropped. The size of ROI was set to 256x256x256.

2.4 Automatic segmentation of aorta and MPA using U-Net

We used five architectures of U-Net and an ensemble method: 2D U-Net, 2D U-Net with pre-trained VGG-16 [16] encoder, 2D U-Net with pre-trained VGG-19 [16] encoder, 2D Attention U-Net [17], and 3D U-Net [13]. The ensemble was performed by majority vote by the above five architectures. These network architectures are shown in Fig. 2. The input size for 2D and 3D U-Net were 256x256 and 256x256x256, respectively. Epoch was set to 40. Mini-batch sizes for 2D and 3D U-Net were set to 4 and 1, respectively. Training and testing processes were performed by 10-fold cross-validation using a mixed dataset of 100 normal cases and 24 CTEPH cases. In the training process, 10% of the training dataset was used for the validation dataset. The network was trained using the Adam optimization algorithm, with Dice loss function, using a single graphical processing unit (NVIDIA GeForce RTX 3090). These network architectures were implemented using TensorFlow [18].

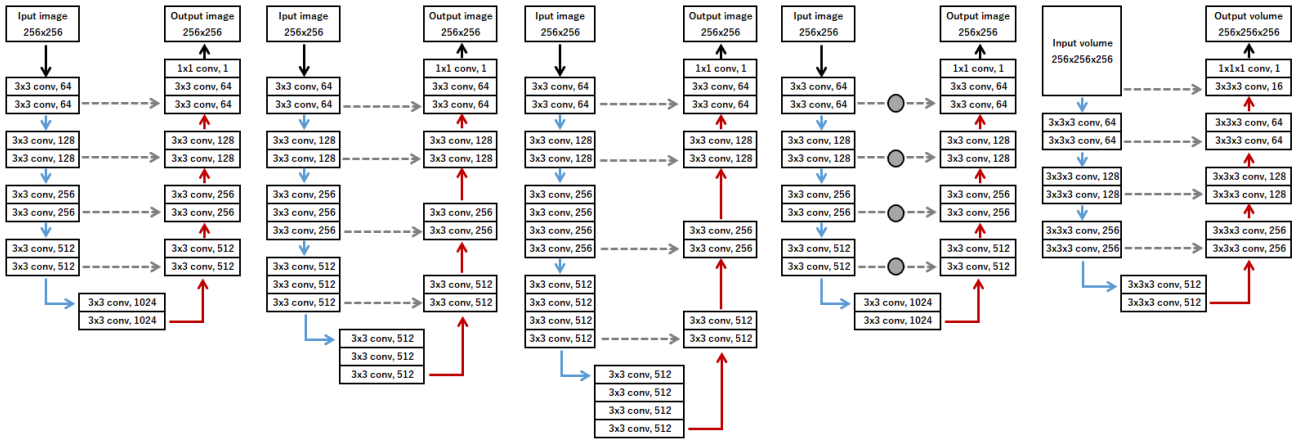

Fig. 2. 2D and 3D U-Net architectures. (a) 2D U-Net, (b) 2D U-Net with pretrained VGG-16 encoder, (c) 2D U-Net with pretrained VGG-19 encoder, (d) 2D attention U-Net, (e) 3D U-Net. Blue, red, and gray lines mean max pooling, transposed convolution, and copy. Black line means input or output. Gray circle means attention gate [17].

3. RESULTS

3.1 Segmentation performance of the aorta and MPA

We evaluated the segmentation performance of seven methods: (a)conventional method [11], (b)2D U-Net, (c)2D U-Net with pre-trained VGG-16 encoder, (d) 2D U-Net with pre-trained VGG-19 encoder, (e)2D attention U-Net, (f)3D U-Net, and (g)the ensemble method of (b) to (f). Dice similarity coefficient (*DSC*) was employed as the evaluation metric. The results are shown in Table 1 and Table 2. These results were compared using pairwise Wilcoxon rank-sum test adjusted by Bonferroni correction. For all vascular parts, 2D U-Nets, 3D U-Net, and the ensemble method achieved significantly higher performance than the conventional method (p-values<0.05). In addition, the ensemble method achieved the highest performance (p-values<0.05).

Table 1 Mean Dice similarity coefficients and standard deviations for segmentation of the aorta and main pulmonary artery of normal cases (dataset A).

		Aortic arch	Ascending aorta	Descending aorta	MPA
(a)	Conventional method [11]	0.952±0.024	0.960±0.013	0.957±0.016	0.935±0.019
(b)	2D U-Net	0.969±0.009	0.978±0.005	0.977±0.004	0.965±0.010
(c)	2D U-Net (VGG-16)	0.967±0.017	0.977±0.006	0.977±0.006	0.962±0.018
(d)	2D U-Net (VGG-19)	0.967±0.014	0.976±0.006	0.976±0.004	0.963±0.016
(e)	2D Attention U-Net	0.969±0.010	0.976±0.006	0.977±0.005	0.962±0.015
(f)	3D U-Net	0.970±0.010	0.977±0.005	0.975±0.005	0.965±0.012
(g)	Ensemble (b～f)	0.973±0.009	0.980±0.004	0.979±0.003	0.969±0.009

Table 2 Mean Dice similarity coefficients and standards deviation for segmentation of the aorta and main pulmonary artery of CTEPH cases (dataset B).

		Aortic arch	Ascending aorta	Descending aorta	MPA
(a)	Conventional method [11]	0.962±0.016	0.960±0.016	0.950±0.019	0.952±0.012
(b)	2D U-Net	0.954±0.051	0.970±0.013	0.971±0.010	0.968±0.009
(c)	2D U-Net (VGG-16)	0.962±0.028	0.969±0.014	0.972±0.010	0.967±0.012
(d)	2D U-Net (VGG-19)	0.968±0.009	0.962±0.035	0.970±0.008	0.966±0.012
(e)	2D Attention U-Net	0.961±0.014	0.967±0.027	0.972±0.008	0.967±0.009
(f)	3D U-Net	0.967±0.011	0.971±0.011	0.968±0.010	0.964±0.008
(g)	Ensemble (b～f)	0.971±0.010	0.975±0.008	0.975±0.006	0.973±0.005

3.2 Evaluation of robustness to the contacts of blood vessels

We focused on the two types of contact parts, (1)contact of the ascending aorta with MPA, (2)contact of the descending aorta with the esophagus. As the evaluation metrics, mean boundary distance (MBD) was employed, which is average of the distances from the boundary of ground truth to the boundary of the segmentation result. The comparison results of the *MBDs* in non-contact and contact boundaries are shown in Table 3 and Table 4. The U-Nets achieved high segmentation performance, whereas the performance significantly decreased in the contact boundaries compared with non-contact boundaries for any methods (p-values<0.05, Wilcoxon rank-sum test). This trend was observed in both of normal and CTEPH cases.

Table 3 Mean boundary distance and standard deviation in the aortic contact parts of normal cases (* p-value<0.05, Wilcoxon rank sum test).

		MBD of ascending aorta (mm)		*MBD* of descending aorta (mm)	
		Non-contact	Contact with MPA	Non-contact	Contact with esophagus
(a)	Conventional method [11]	0.667±0.530	0.715±0.529*	0.522±0.364	0.617±0.501*
(b)	2D U-Net	0.346±0.110	0.487±0.262*	0.285±0.086	0.411±0.232*
(c)	2D U-Net (VGG-16)	0.333±0.109	0.497±0.270*	0.277±0.092	0.436±0.258*
(d)	2D U-Net (VGG-19)	0.328±0.111	0.493±0.261*	0.279±0.089	0.413±0.243*
(e)	2D Attention U-Net	0.337±0.124	0.507±0.289*	0.279±0.086	0.415±0.235*
(f)	3D U-Net	0.329±0.096	0.543±0.350*	0.291±0.084	0.504±0.341*
(g)	Ensemble (b～f)	0.301±0.090	0.419±0.219*	0.260±0.072	0.376±0.210*

Table 4 Mean boundary distance and standard deviation in the aortic contact parts of CTEPH cases (* p-value<0.05, Wilcoxon rank sum test).

		MBD of ascending aorta (mm)		*MBD* of descending aorta (mm)	
		Non-contact	Contact with MPA	Non-contact	Contact with esophagus
(a)	Conventional method [11]	0.483±0.302	0.958±0.632*	0.461±0.268	0.846±0.476*
(b)	2D U-Net	0.345±0.129	0.626±0.390*	0.292±0.104	0.479±0.348*
(c)	2D U-Net (VGG-16)	0.354±0.154	0.610±0.374*	0.288±0.092	0.439±0.285*
(d)	2D U-Net (VGG-19)	0.363±0.148	0.618±0.336*	0.300±0.105	0.444±0.330*
(e)	2D Attention U-Net	0.346±0.146	0.615±0.347*	0.292±0.092	0.456±0.295*
(f)	3D U-Net	0.347±0.142	0.747±0.486*	0.303±0.093	0.542±0.312*
(g)	Ensemble (b～f)	0.318±0.131	0.545±0.252*	0.266±0.080	0.439±0.257*

Fig. 3 shows the relations of the *MBD* and *CSR* for 2D U-Net, 3D U-Net, and the ensemble method. The *MBDs* were increased as the *CSR* increased. For CTEPH cases, the contact boundaries caused substantially lower segmentation performances. Examples of the aortic segmentation results of a CTEPH case are shown in Fig. 4. It is difficult to determine the correct boundary because of the contact of the ascending aorta and MPA, however, some U-Net architectures achieved almost accurate segmentation. A method for the ensemble using advantages of the network architectures would be developed in the future.

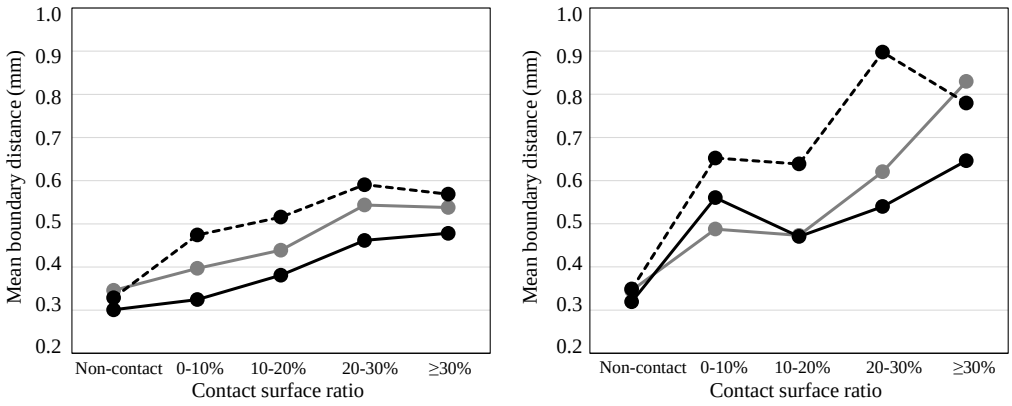

Fig 3 Relation of mean boundary distance and contact surface ratio for contacts of the ascending aorta with main pulmonary artery in (a) normal and (b) CTEPH cases. Black and gray lines show an ensemble method and 2D U-Net. Black dashed line shows 3D U-Net.

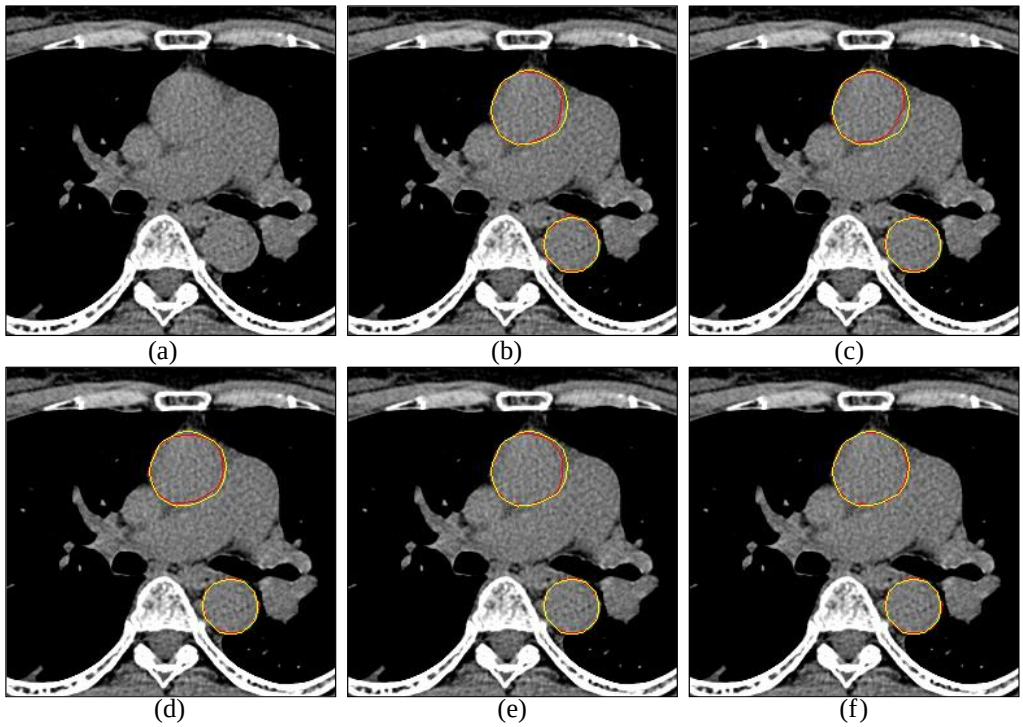

Fig 4 Segmentation results of the aorta using U-Net. Red and yellow boundaries are an automatic segmentation result and ground truth, respectively. (a) A cropped CT image (*CSR* of the ascending aorta and MPA is 30%), (b) 2D U-Net (*MBD* in the contact part of the ascending aorta: 1.20mm), (c) 2D U-Net with pre-trained VGG-16 encoder (*MBD*: 1.46mm), (d) 2D U-Net with pre-trained VGG-19 encoder (*MBD*: 0.83mm), (e) 2D attention U-Net (*MBD*: 0.68mm), (f) 3D U-Net (*MBD*: 0.44mm).

4. CONCLUSIONS

We applied U-Net to the segmentation of the aorta and MPA from non-contrast CT images for normal and chronic thromboembolic pulmonary hypertension (CTEPH) cases. Furthermore, we evaluated their robustness to the contacts of the blood vessels. The aorta and MPA segmentation methods using these U-Net achieved higher performance than a conventional method. Although the contact boundaries of blood vessels caused lower performance compared with the non-contact boundaries, the mean boundary distances were below about one pixel.

ACKNOWLEDGEMENT

This work was supported by JSPS KAKENHI Grant Number 19K12784, and by the SECOM Science and Technology Foundation.

REFERENCES

[1] Tan, R. T., Kuzo, R., Goodman, L. R., Siegel, R., Haasler, G. R., Presberg, K., "Utility of CT scan evaluation for predicting pulmonary hypertension in patients with parenchymal lung disease", Chest, 113(5), 1250-1256 (1998).
[2] Edwards, P. D., Bull, R. K., Coulden, R., "CT measurement of main pulmonary artery diameter", Br. J. Radiol., 71(850), 1018-1020 (1998).
[3] Lange, T. J., Dornia, C., Stiefel, J., Stroszczynski, C., Arzt, M., Pfeifer, M., Hamer, O. W., "Increased pulmonary artery diameter on chest computed tomography can predict borderline pulmonary hypertension", Pulmonary Circulation, 3(2), 363-368 (2013).
[4] Corson, N., Armato III, S. G., Labby, Z. E., Corson, N., Armato III, S. G., Labby, Z. E., Straus, C., Starkey, A., Gomberg-Maitland, M., "CT-Based Pulmonary Artery Measurements for the Assessment of Pulmonary Hypertension", Acad. Radiol., 21(4), 523-530 (2014).
[5] Kurugol, S. Estepar, R. S. J. Ross, J. and Washko, G. R. "Aorta segmentation with a 3D level set approach and quantification of aortic calcifications in non-contrast chest CT," in Annual Int. Conf. of the IEEE, 2343-2346 (2012).
[6] Kurugol, S. Come, C. E. Diaz, A. A. Ross, J. C. Kinney, G. L. Black-shinn, J. L. Hokanson, J. E. Budoff, M. J. Washko, G. R. and Estepar, R. S. J. "Automated quantitative 3D analysis of aorta size, morphology, and mural calcification distributions," Med. Phys. 42(9), 5467-5478 (2015).
[7] Xie, Y. Padgett, J. Biancardi, A. M. and Reeves, A. P. "Automated aorta segmentation in low-dose chest CT images," Int. J. CARS 9(2), 211-219 (2014).
[8] Xie, Y. Liang, M. Yankelevitz, D. F. Henschke, C. I. and Reeves, A. P. "Automated measurement of pulmonary artery in low-dose non-contrast chest CT images," Proc. SPIE 9414, 9414G (2015).
[9] Gamechi, Z. S., Arias-Lorza, A. M., Pedersen, J. H., Bruijne, M., "Aorta and pulmonary artery segmentation using optimal surface graph cuts in non-contrast CT", Proc SPIE 10574, 105742D (2018).
[10] Gamechi, Z. S., Bons, L. R., Giordano, M., Bos, D., Budde, R. P. J., Kofoed, K. F., Pedersen, J. H., Ross-Hesselink, J. W., Bruijne, M., "Automated 3D segmentation and diameter measurement of the thoracic aorta on non-contrast enhanced CT", Eur. Radiol. 29(9),4613-4623 (2019).
[11] Suzuki, H., Kawata, Y., Niki N., Sugiura, T., Tanabe, N., Kusumoto, M., Eguchi, K., Kaneko, M., "Automated assessment of aortic and main pulmonary arterial diameters using model-based blood vessel segmentation for predicting chronic thromboembolic pulmonary hypertension in low-dose CT lung screening", Proc SPIE 10575, 105750X (2018).
[12] Ronneberger, O., Fischer, P., Brox, T., "U-net: Convolutional networks for biomedical image segmentation," MICCAI 2015, 234-241 (2015).
[13] Çiçek, Ö., Abdulkadir, A., Lienkamp, SS., Brox, T., and Ronneberger, O., "3D U-Net: Learning dense volumetric segmentation from sparse annotation", MICCAI 2016, 424-432 (2016).
[14] Kanazawa, K. Kawata, Y. Niki, N. Satoh, H. Ohmatsu, H. Kakinuma, R. Kaneko, M. Moriyama, N. and Eguchi, K. "Computer-aided diagnosis for pulmonary nodules based on helical CT images," Comput. Med. Imaging Graph. 22(2), 157-167 (1998)
[15] Yoneda, K. Matsuhiro, M. Suzuki, H. Kawata, Y. Niki, N. Nakano, Y. Ohmatsu, H. Kusumoto, M. Tsuchida, T. Eguchi, K. Kaneko, M. "Computer-aided diagnosis for osteoporosis using chest 3D CT images," Proc. of SPIE 9785, 97853A (2016)
[16] Simonyan, K., Zisserman, A., "Very Deep Convolutional Networks for Large-Scale Image Recognition", arXiv, 1409.1556 (2014).
[17] Oktay, O., Schlemper, J., Folgoc, L. L., Lee, M., Heinrich, M., Misawa, K., Mori, K., McDonagh, S., Hammerla, N. Y., Kainz, B., Glocker, B., Rueckert, D., "Attention U-Net: Learning Where to Look for the Pancreas", arXiv, 1804.03999 (2018).
[18] Abadi, M., Barham, P., Chen, J., Chen, Z, Davis, A., Dean, J., Devin, M., Ghemawat, S., Irving, G., Isard, M., Kudlur, M., Levenberg, J., Monga, R., Moore, S., Murray, D. G., Steiner, B., Tucker, P., Vasudevan, V., Warden, P,., Wicke, M., Yu, Y., and Zheng, X., "Tensorflow: A system for large-scale machine learning", 12th USENIX symposium on operating systems design and implementation, 265-283 (2016).